https://doi.org/10.3311/PPtr.38258

Periodica Polytechnica Transportation Engineering, 53(3), pp. 267–276, 2025

Effects of Location and Height of Vortex Generators on Aerodynamic Performance of NACA 4412 Airfoil

Dénes Ágoston Solnay[1*], József Molnár[1], István Lakatos[1]

[1] Department of Automotive and Railway Engineering, Audi Hungaria Faculty of Automotive Engineering, Széchenyi István University, Egyetem tér 1., H-9026 Győr, Hungary
[*] Corresponding author, e-mail: solnay.d.agoston@gmail.com

Received: 13 September 2024, Accepted: 14 April 2025, Published online: 24 April 2025

Abstract

This study focuses on the aerodynamic effect of vortex generators (VGs) placed on the wing surface, with a focus on the height and chordwise position of the VGs. NACA 4412 airfoil was used for the investigation, which is a frequently used and well-researched airfoil in the aerospace industry, with a chord length (c) of 200 mm. Six different configurations have been analyzed with Computational Fluid Dynamics (CFD), with three chordwise positions (x) and two trailing edge heights (h). The results showed that VGs placed furthest from the leading edge (x/c = 20%) were able to increase lift and reduce drag to the greatest extent. In terms of height, the shorter (h/c = 0.5%) VGs produced the most lift. These results provide valuable insights as to how vortex generator design can be optimized for aerodynamic performance across various operating conditions.

Keywords

vortex generator, boundary layer separation, flow separation control, Computational Fluid Dynamics, aerodynamics

1 Introduction

In fluid mechanics, boundary layer refers to the region of flow near a solid surface, where friction is dominant and in which velocity changes from zero at the solid surface to the freestream value (Benson, 2021). When the boundary layer detaches from the surface, it is called flow separation or boundary layer separation. This is a critical condition for various engineering systems because it causes a loss of lift, an increase in drag, and vibration (Zhang et al., 2023).

One of the most used methods of flow separation control is the use of vortex generators (VGs), which are small plates mounted on the suction side of the wing. A vortex generator creates vortices that transfer air with high energy and momentum from the freestream flow into the boundary layer, thereby energizing it (Houghton et al., 2016). This increases lift and reduces drag around curved surfaces like wings.

VGs are widely used in aviation, for example, to reduce the drag of helicopters (Gibertini et al., 2015), wing-on-ground craft fuselages (Methal et al., 2023) or increase the lift on wings (Himo et al., 2021). In the automotive industry, VGs are mainly used on racing cars, as these vehicles often feature wings. In motorsports, increasing downforce, rather than lift, is important. VGs are widely used on wings to create higher downforce values, as well as under the car in the Venturi tunnels (Katz, 2021). VGs are also used on road cars and high-speed trains, to reduce drag (Li et al., 2023). VGs are also used in the energy sector to improve the flow around wind turbine blades (De Tavernier et al., 2021) or increase heat transfer of heat exchangers (Priyadi et al., 2022) and solar chimneys (Sheikhnejad and Gandjalikhan Nassab, 2021).

To design a properly working VG, the trailing edge height (h) and chordwise distance from the leading edge (x) are critical design parameters. The correct choice of these parameters can increase the lift of the wing, reduce the drag and increase the stall angle. Dividing these parameters by the chord length (c), h/c and x/c dimensionless numbers can be examined. Mueller-Vahl et al. (2013) found that the optimal chordwise position of the vortex generators is in the range of x/c = 15–20%. Li et al. (2020), De Tavernier et al. (2021) and Balaji et al. (2023) all concluded that the optimal location is at 20%, however, Zhang et al. (2016) found that at 10% of chord the maximum lift coefficient is highest. Based on these, x/c = 10%, 15%, and 20% were investigated during this research. Gao et al. (2015) and Zhang et al. (2016) both kept their h/c ratio under 1%, accordingly 0.5% and 0.75% were used in this study.

Cite this article as: Solnay, D. Á., Molnár, J., Lakatos, I. (2025) "Effects of Location and Height of Vortex Generators on Aerodynamic Performance of NACA 4412 Airfoil", Periodica Polytechnica Transportation Engineering, 53(3), pp. 267–276. https://doi.org/10.3311/PPtr.38258

The aim of the research is to find the x/c and h/c geometrical ratios that achieve the highest lift coefficient and the lowest drag coefficient values with constant Reynolds number at various angles of attacks (AoA). Computational Fluid Dynamics was used for the investigation.

2 Flow separation and vortex generators

A wing placed in the flow generates lift by causing the airflow to curve around the wing, creating a pressure differential between the upper and lower surfaces of the wing. Pressure is highest at the stagnation point and, as the air moves downstream on the upper surface, the flow velocity increases until it reaches point M, where the flow velocity is maximum and pressure gradient $\partial p/\partial x$ is zero. After point M, pressure increases, until the velocity gradient $\partial U/\partial y$ becomes zero at the separation point S (Rohács et al., 2012) (Fig. 1).

This is followed by having reverse flow close to the surface of the wing, an increase in pressure, and ultimately a decrease in lift and an increase in drag.

As the air in the boundary layer is moving slower, it contains less energy and less momentum than the faster freestream flow. When this faster air doesn't continue to follow the curvature of the wing surface, it causes the boundary layer to separate. VGs can prevent flow separation, by creating vortices. These vortices, as they rotate and swirl the air, help mix the high energy freestream flow with the boundary layer, transferring enough energy for it to stay attached to the surface. The process of getting momentum and energy into the boundary layer from the freestream air is a form of momentum transfer.

3 Vortex generator geometry

In this study, the base of the investigation was a NACA 4412 wing profile, with a chord length of c = 200 mm.

Different triangular-shaped VGs were used to improve the aerodynamical properties of this profile (Fig. 2). 2 geometrical parameters were investigated with 6 geometries:

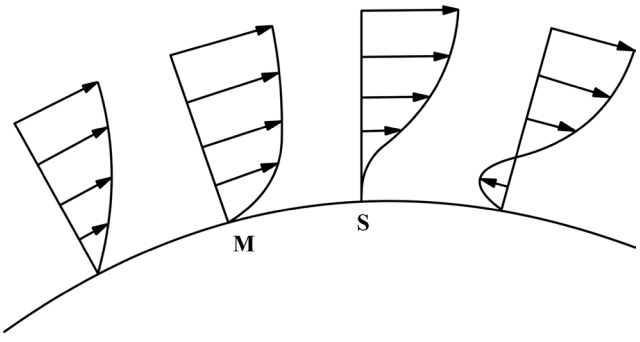

Fig. 1 Boundary layer separation

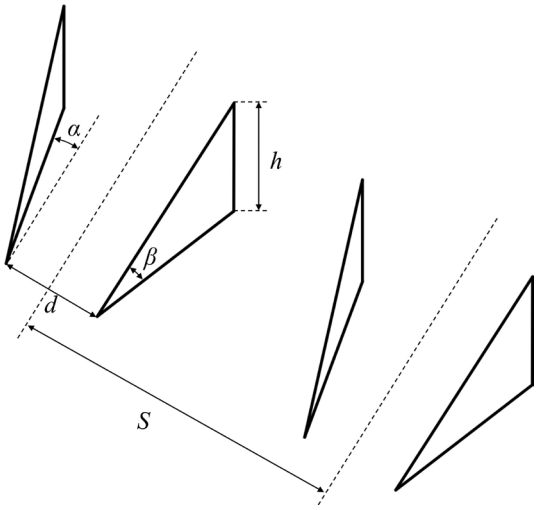

Fig. 2 Sketch of VGs

the distance of the VGs from the leading edge in the chordwise direction (x) and the height of the vortex generators' trailing edge (h). All other parameters were kept constant.

In this study, x/c = 10%, 15%, and 20% were investigated, with h/c = 0.5% and 0.75%. Table 1 summarizes the geometrical parameters of the VGs of this study.

For all cases the leading edge spacing d = 8 mm, spacing of adjacent pairs of VGs S = 40 mm, vortex generator AoA α = 14° and leading edge angle β = 14°.

4 Simulation methods

ANSYS Fluent finite volume Computational Fluid Dynamics software was used for the analysis, and ANSYS Fluent meshing for the meshing (Ansys, online).

4.1 Turbulence modeling

Turbulent flow refers to an unsteady flow characterized by the random and irregular movement of fluid elements. (Anderson and Cadou, 2023). In the Fluent solver, the Reynolds-averaged Navier-Stokes (RANS) equations were employed to model the turbulent flow, utilizing the k-ω SST two-equation eddy-viscosity turbulence model. Near the wall, this turbulence model uses the

Table 1 Vortex generator configuration parameters

Vortex generator ID	Chordwise length x (mm)	Trailing edge height h (mm)
VG1	20	1
VG2	30	1
VG3	40	1
VG4	20	1.5
VG5	30	1.5
VG6	40	1.5

k-ω turbulence model, since that doesn't involve complex non-linear near-wall damping functions, which are required for the k-ε model. However, k-ω is more sensitive to freestream conditions, so the numerically robust k-ε is utilized in the freestream flow. This means that the k-ω SST turbulence model combines the advantages of both k-ω and k-ε models, so it accurately captures complex turbulent behavior (Ansys, 2021).

4.2 Simulation setup and boundary conditions

Steady state and incompressible flow were assumed for all the calculations. In the case of incompressibility, the density is assumed to be constant, and the conservation of mass and conservation of momentum equation reduces to:

$$\nabla \times \boldsymbol{u} = 0, \tag{1}$$

$$\boldsymbol{u} \times \nabla \boldsymbol{u} - \nabla \times \left(\nu \nabla \boldsymbol{u}\right) = -\nabla p, \tag{2}$$

where $\boldsymbol{u}$ is the fluid velocity vector, ν is the kinematic viscosity and p is the kinematic pressure (Ansys, 2021).

Air was maintained at constant density and viscosity corresponding to 15 °C, and an operational pressure of 101,325 Pa, which is the International Standard Atmosphere (ISA) condition.

A 200 mm chord length NACA 4412 profile was used for the calculations, which was 600 mm spanwise (b). The air domain is a combination of a prism with a semi-circular cross-section (with a rotational axis as the wing's leading edge) and a cuboid. The 2 sides of the air domain were symmetry boundary conditions. As all simulations were conducted at Re = 4×10^5 and modeling at ISA condition, the inlet velocity can be calculated as:

$$U = \frac{\mathrm{Re} \times \mu}{\rho \times c} \approx 21.2147\,\mathrm{m/s}, \tag{3}$$

where Re represents the Reynolds number and μ is the dynamic viscosity of the air.

In this research, a range of AoA values at constant Reynolds number were investigated for each geometry, 0°, 2°, 4°, 6°, 8°, 10°, 12°, 13°, 14°, 15° and 16°. By having 6 different vortex generator geometries, and a case without any vortex generators (clear model) was also examined, a total of 77 individual CFD simulations were performed (Fig. 3).

4.3 Lift and drag calculations

To change the AoA without having to change the geometry, the inlet velocity x and y components were changed

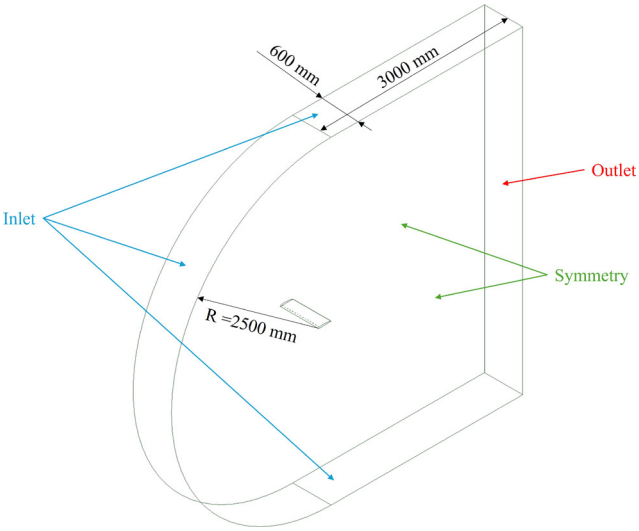

Fig. 3 CFD domain

between simulation cases, and the air domain x and y force components (F_x and F_y) were calculated. Then these force components could be calculated into lift (L) and drag (D):

$$L = F_y \cos\left(\mathrm{AoA}\right) - F_x \sin\left(\mathrm{AoA}\right), \tag{4}$$

$$D = F_y \sin\left(\mathrm{AoA}\right) + F_x \cos\left(\mathrm{AoA}\right). \tag{5}$$

Lift- and drag coefficients can be calculated as:

$$c_L = \frac{2L}{\rho U^2 A}, \tag{6}$$

$$c_D = \frac{2D}{\rho U^2 A}, \tag{7}$$

where Eq. (8) is the frontal area:

$$A = b \times c = 0.6\ \mathrm{m} \times 0.2\ \mathrm{m} = 1.2\ \mathrm{m}^2. \tag{8}$$

5 Numerical mesh and mesh independence study

To ensure the accuracy of the simulation results, a mesh independence study was conducted with 6 different numerical meshes for the same geometry. This investigation is necessary to determine the density of the mesh and optimize the computational efficiency of the numerical grid. A baseline mesh of 1.98 million cells was used, and different parameters of this mesh were varied, together and separately to create the 6 different numerical grids. The calculation of aerodynamic forces is important for this study, so the quality of the surface mesh is crucial. For this reason, the finest mesh was created by refining all surface mesh parameters by 25% to the baseline mesh. Furthermore, the maximum edge size for the wing's surface (which is important in the middle of

the wing, where there is no significant curvature) and the inflation layer first layer height and number of layers (with constant total thickness) were investigated, to ensure better efficiency. Since the difference between the finest and base mesh lift coefficient results was 2.62% (Fig. 4) and 2.33% difference in drag coefficient (Fig. 5), this 1.98 million baseline mesh was used for the rest of the calculation. In this study, we aimed for $y^+ = 1$ to ensure the proper resolution of the boundary layer, and with the baseline mesh the average y^+ value was 0.83.

Poly-Hexcore cells were used for the volume mesh. This meshing approach fills the bulk region with hexahedral elements to reduce computational time, layered polyprism cells in the boundary layer, and connects these two regions with general polyhedral elements, which are suitable for complex geometries (Ansys, 2020).

6 Simulation results

Table 2 and Table 3 contain the lift and drag coefficient results of the CFD simulations.

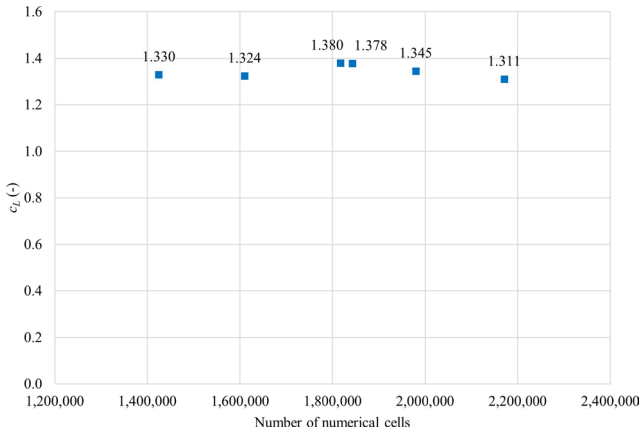

Fig. 4 Lift coefficient values of the different meshes

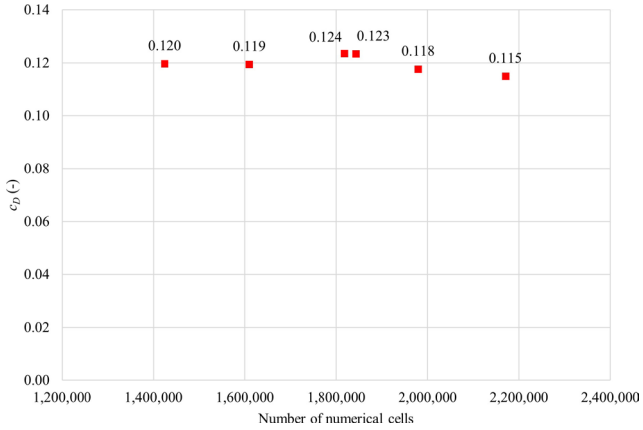

Fig. 5 Drag coefficient values of the different meshes

6.1 Clear model results and expectations

As Fig. 6 shows, the drag coefficient increases over the whole investigated AoA range.

Lift coefficient is growing at a nearly linear rate from AoA = 0° to 12°, beyond that, the rate of increase begins to level off, reaching its peak at 15°. After this point, the lift coefficient declines (Fig. 7).

An important requirement for a VG to work properly is to be positioned before the separation point to give it enough space and time to put energy and momentum into the boundary layer to help delay separation. Therefore, it is worthwhile examining the clear model to determine the chordwise length (x) value at which the velocity gradient ($\partial U/\partial y$) at the wall first becomes zero (Fig. 8). When the velocity gradient is zero, the wall shear stress is also zero, which can be queried in Fluent.

At AoA = 0° and 2° separation never occurred. As Fig. 8 shows, the separation point did not decrease below x = 40 mm even at a 16° AoA, therefore all 6 vortex generator configurations are located before the clear model's separation point.

Since this method of delaying separation and increasing lift requires transferring momentum from the freestream air to the boundary layer, the vortex generator needs to be higher than the local boundary layer thickness (Katz, 1996).

6.2 Vortex generator cases

At lower angles of attack, all six VG configuration performed worse than the clear model, since all generated less lift up to AoA = 10°. VGs mix the boundary layer and the freestream flow, which increases the total amount of kinetic energy loss. So, when there is no significant flow separation, VGs don't tend to have added benefits.

The comparison of the h = 1 mm (h/c = 0.5%) vortex generator configuration (VG1, VG2, VG3) with the clear model above AoA = 12° (Fig. 9 (b) and Fig. 10 (b)) shows that all three VGs produced more lift than the clean model, with the maximum lift $c_{L\max}$ being reached at 15°. Up to 15°, VG3 generated the largest increase in lift compared to the clear model, while VG1 generated the smallest. This means that the vortex generator farthest from the leading edge downstream (x/c = 20%) produced the most lift, and the closest one (x/c = 10%) produced the least. The same trend is true for the three h = 1.5 mm (h/c = 0.75%) configurations, as VG6 generated the most lift for angles of attack higher than 4°, and VG4 the least (Fig. 9 (c)). After

Table 2 Lift coefficient simulation results

	Lift coefficient c_L (–)						
AoA	Clear model	VG1	VG2	VG3	VG4	VG5	VG6
0	0.379	0.377	0.377	0.376	0.376	0.375	0.374
2	0.573	0.571	0.570	0.570	0.568	0.567	0.566
4	0.758	0.754	0.753	0.754	0.750	0.750	0.750
6	0.929	0.923	0.923	0.924	0.919	0.919	0.919
8	1.080	1.075	1.075	1.076	1.069	1.070	1.070
10	1.215	1.213	1.213	1.214	1.209	1.209	1.210
12	1.344	1.345	1.346	1.349	1.340	1.343	1.346
13	1.374	1.377	1.379	1.383	1.370	1.375	1.379
14	1.385	1.392	1.394	1.399	1.385	1.391	1.396
15	1.386	1.396	1.397	1.405	1.389	1.396	1.403
16	1.366	1.368	1.376	1.376	1.360	1.371	1.380

Table 3 Drag coefficient simulation results

	Drag coefficient c_D (–)						
AoA	Clear model	VG1	VG2	VG3	VG4	VG5	VG6
0	0.0285	0.0282	0.0282	0.0284	0.0283	0.0284	0.0286
2	0.0325	0.0322	0.0323	0.0324	0.0324	0.0325	0.0327
4	0.0402	0.0398	0.0399	0.0400	0.0400	0.0401	0.0403
6	0.0514	0.0510	0.0510	0.0511	0.0512	0.0512	0.0514
8	0.0667	0.0663	0.0662	0.0664	0.0666	0.0666	0.0667
10	0.0876	0.0874	0.0873	0.0873	0.0881	0.0879	0.0880
12	0.1181	0.1177	0.1173	0.1174	0.1183	0.1180	0.1178
13	0.1328	0.1321	0.1317	0.1318	0.1325	0.1322	0.1322
14	0.1482	0.1472	0.1468	0.1467	0.1476	0.1472	0.1470
15	0.1654	0.1639	0.1642	0.1630	0.1645	0.1636	0.1633
16	0.1981	0.2015	0.2000	0.2005	0.2023	0.2017	0.1992

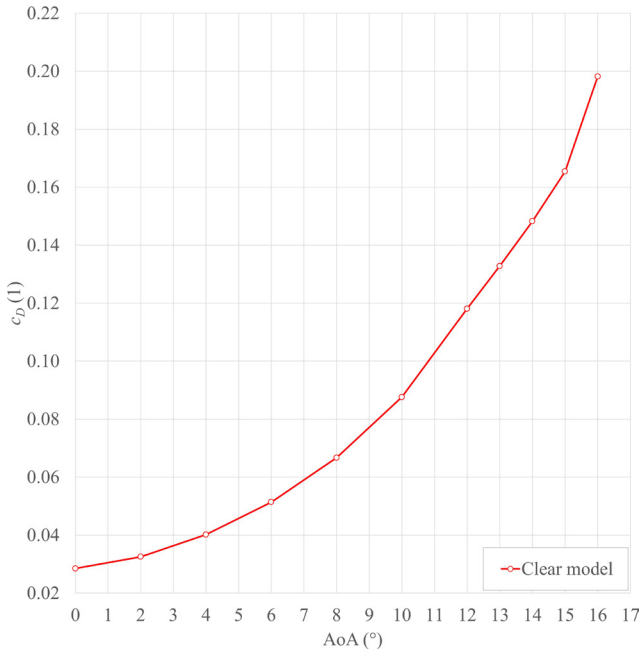

Fig. 6 Clear model drag coefficient values

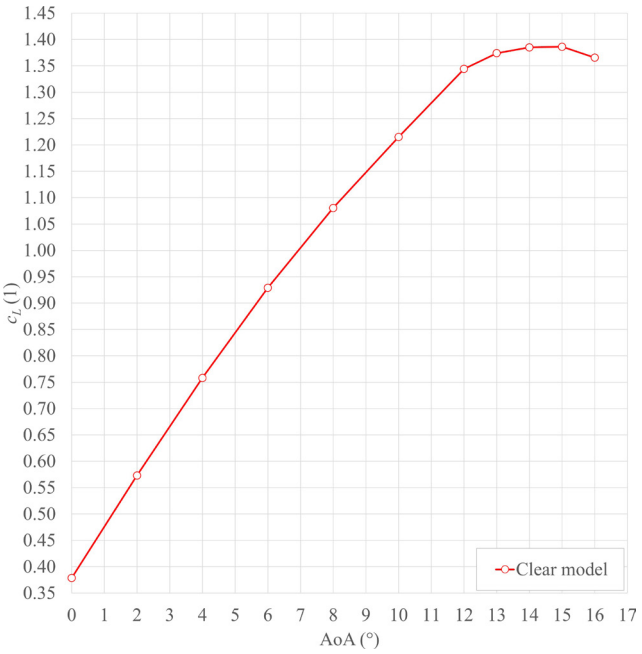

Fig. 7 Clear model lift coefficient values

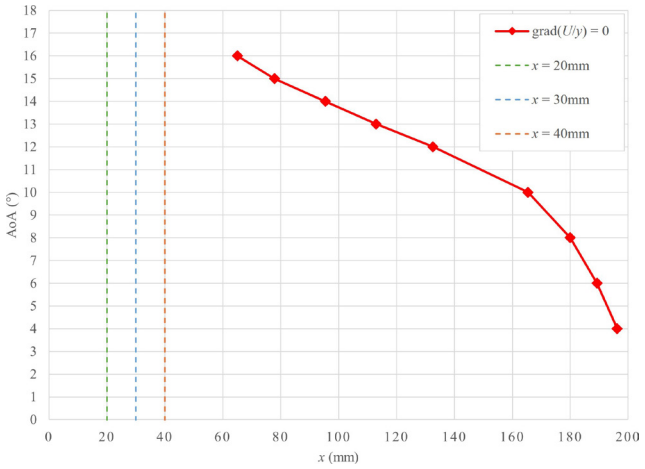

Fig. 8 Separation line of the clear model

the maximum lift coefficient (AoA = 15°), all VGs experienced a decrease in lift.

At 16°, VG2 and VG3 produced similar results in lift, as VG3 experienced a significant decrease in lift. This drop at higher AoA was caused by the local boundary layer thickness being too large for the 1 mm trailing edge height to induce significant mixing between the freestream flow and the boundary layer. At x = 20 mm and 30 mm, the boundary layer is thinner, allowing the same trailing edge height to facilitate adding more momentum and kinematic energy from the freestream flow to the boundary layer, than at x = 40 mm. Since VG6 has a greater trailing edge height than VG3 for the same x location, it can facilitate higher mixing of layers (Fig. 11).

However, VG2 and VG3 generate more lift at high AoA than VG1, regardless of their distance from the leading edge. The reason why putting VGs further downstream is more efficient is that the swirl that the VGs create in the air dissipates in strength over distance, and if they are located too far upstream, they lose their usefulness by the time they are needed the most.

When the VGs are placed further downstream, the swirl is introduced (mixing the BL with high energy flow) closer to the separation zone. Consequently, the point of separation can be delayed. Furthermore, VGs create stagnation zones ahead of them, which decreases the suction on the upper side of the wing. Since the strongest suction occurs just after the leading edge, these stagnation zones will have a greater effect at lower x values (Fig. 12).

The larger a VG (bigger h), the larger the stagnation zone it creates, which results in less lift (Fig. 12). This is the reason why VGs with a trailing edge height of 1.5 mm came with lower lift compared to those with 1 mm. The bigger VGs cause slightly bigger stagnation pressure ahead of them, which increases pressure on the suction side of the wing and ultimately loss of lift, as explained earlier.

In drag, until AoA = 15° all three VGs with a trailing edge height of 1 mm resulted in lower drag values. In the same AoA region, some of the 1.5 mm VGs generated more drag (Fig. 10 (a)). The reason behind this is that the positive effect of delaying flow separation was equalized by the added skin-friction drag, due to the bigger surface of the VGs. This added friction was not so overwhelming for the smaller VGs. Furthermore, due to the thickness of a VG, there is an added pressure drag component, because flow separates, and a wake region forms at the VG trailing edge (Fig. 13).

At 16° of AoA, the local boundary layer thickness is too large for the VGs to decrease the total drag by delaying the separation (Fig. 11), but there is the added viscous drag and pressure drag due to the thickness of the VGs. Due to the reasons above, for both the 1 mm and 1.5 mm VG configurations, the x = 20 mm generated the most drag (Fig. 10 (b) and Fig. 10 (c)).

7 Conclusion

In this paper, the aerodynamic effect of the chordwise length and trailing edge height of vortex generators were investigated on the NACA 4412 airfoil, at 4 × 10^5 Re. The conclusion was that vortex generators with smaller trailing edge heights (h/c = 0.5%) performed better in terms of lift generation at lower angles of attack than 15°, generating higher maximum lift coefficient values. In drag, the ones positioned further from the wing's leading edge (x/c = 20%) resulted in lower drag.

Based on the investigation, the optimal vortex generator position was x/c = 20% (VG3 and VG6) for increasing lift and decreasing drag. VG3 (h/c = 0.5%, x/c = 20%) was the best to generate the most amount of lift and least amount of drag until 15° of AoA and reaching the highest peak in lift. However, at maximum AoA (16°), VG6 (h/c = 0.75%, x/c = 20%) could generate the most lift and least drag out of all the vortex generator configurations.

The mesh resolution used in this study, although computationally efficient, cannot adequately model smaller-scale turbulence effects. To address this, more accurate simulation results could be obtained in the future using a finer

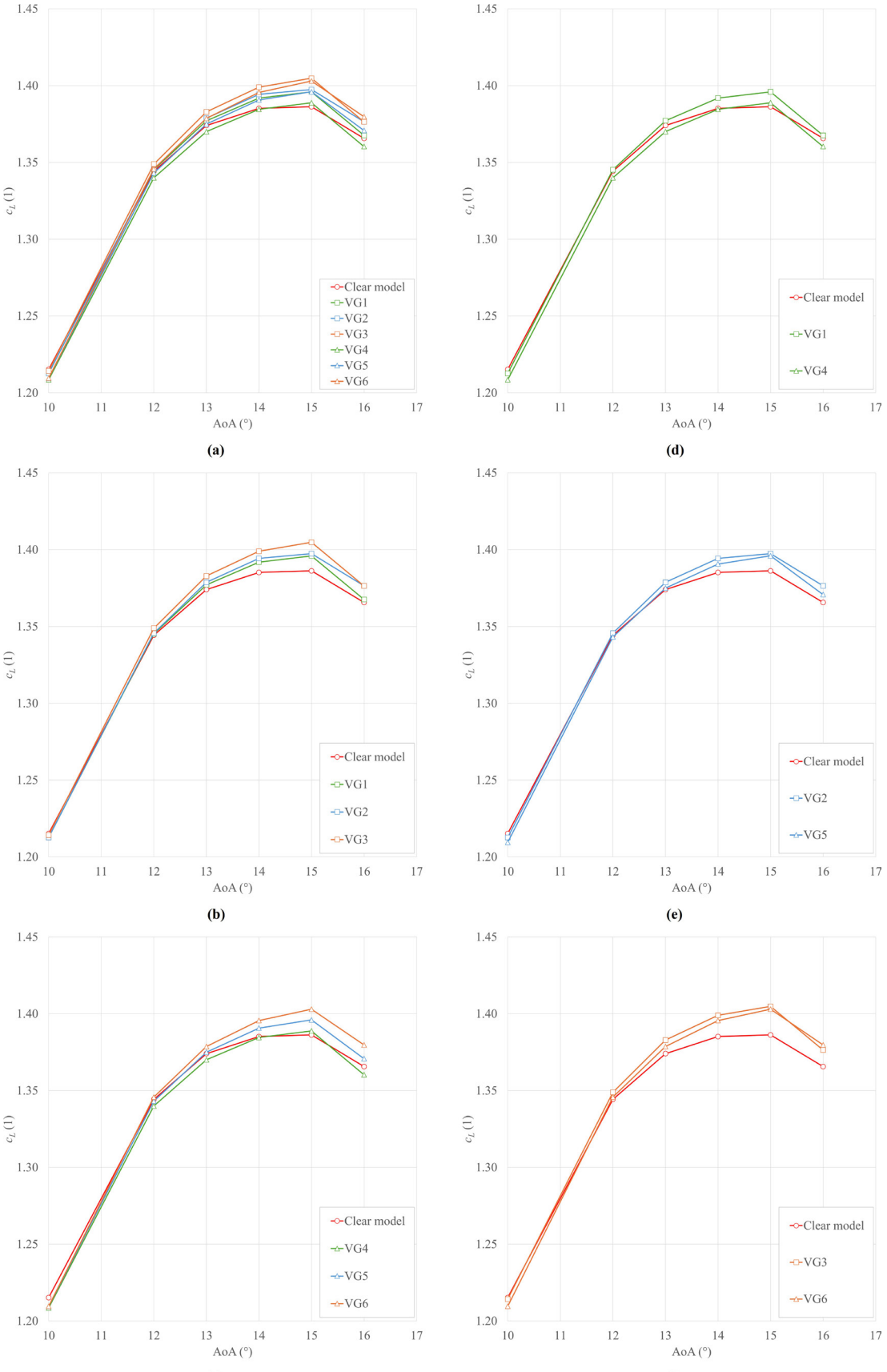

Fig. 9 Lift coefficient simulation results of the clear model compared with the VGs between 10° and 16° AoA: (a) all VGs, (b) h = 1 mm VGs, (c) h = 1.5 mm VGs, (d) x = 20 mm VGs, (e) x = 30 mm VGs, (f) x = 40 mm VGs

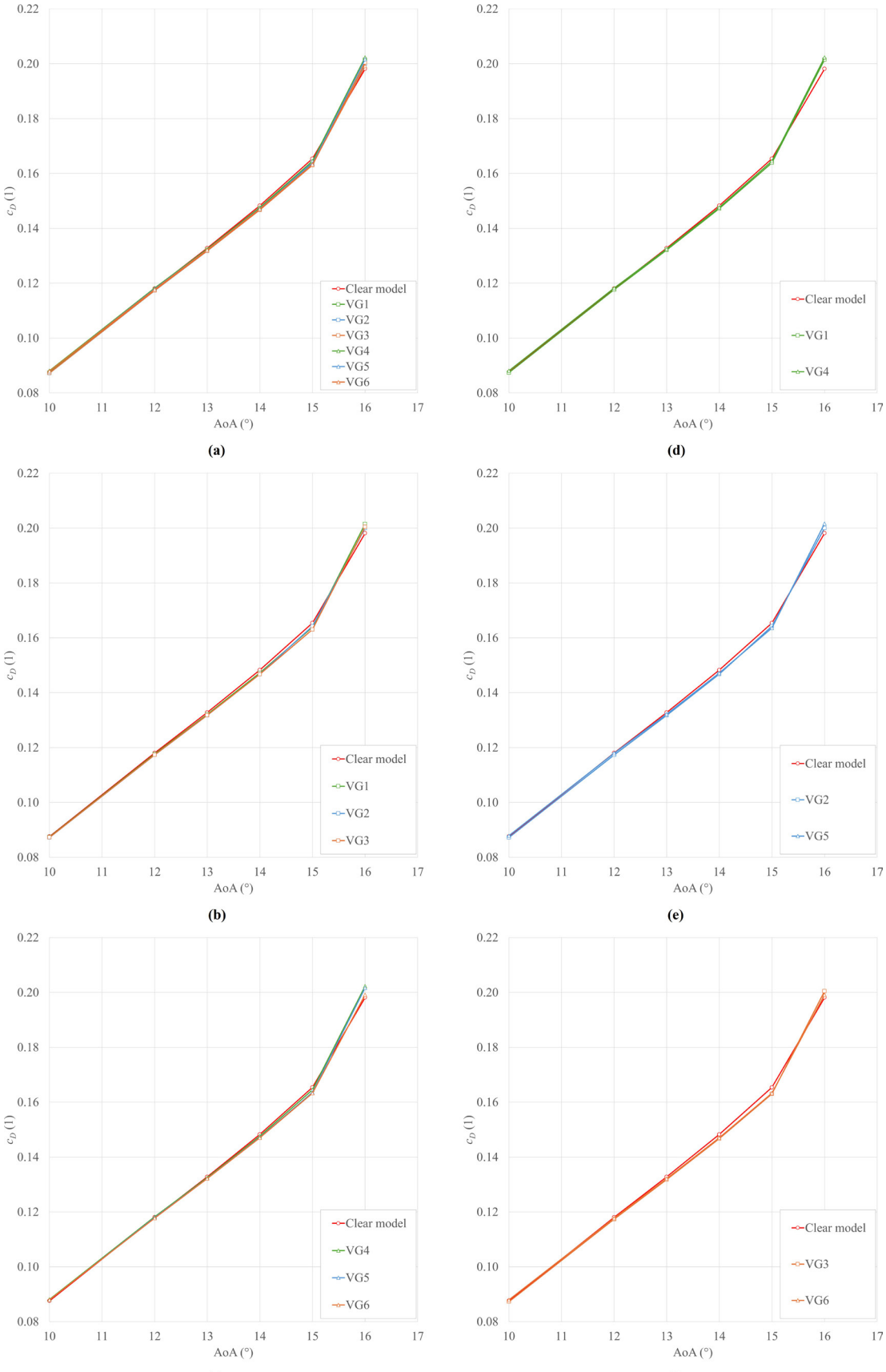

Fig. 10 Drag coefficient simulation results of the clear model compared with the VGs between 10° and 16° AoA: (a) all VGs, (b) h = 1 mm VGs, (c) h = 1.5 mm VGs, (d) x = 20 mm VGs, (e) x = 30 mm VGs, (f) x = 40 mm VGs

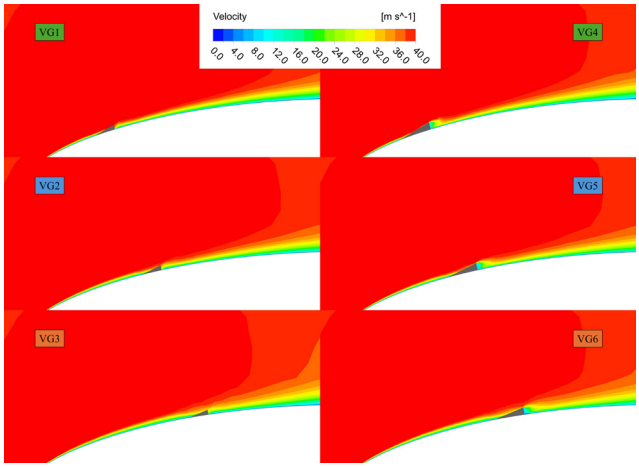

Fig. 11 All VGs boundary layer velocity contour plot at AoA = 16°

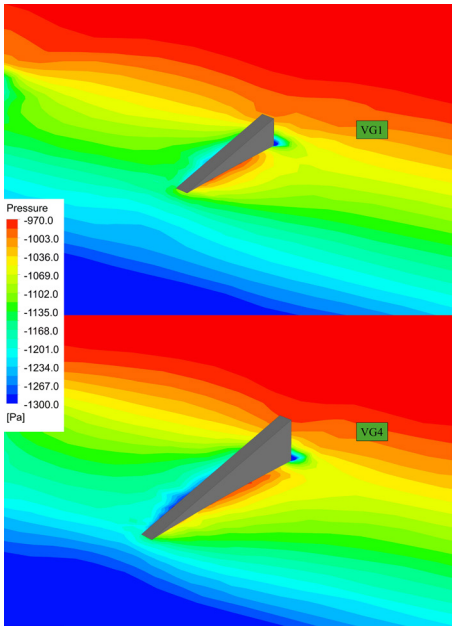

Fig. 12 VG1 and VG4 pressure contour plot at AoA = 14°

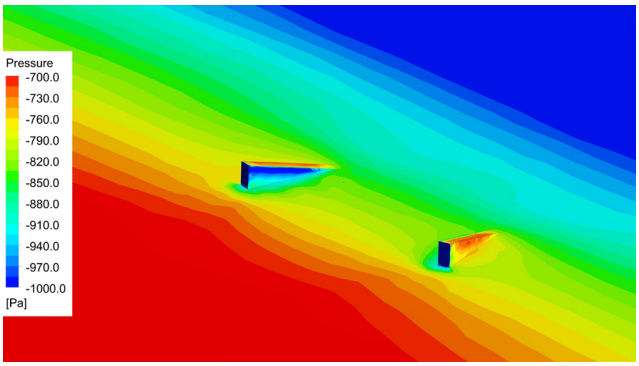

Fig. 13 VG3 pair pressure contour plot at AoA = 16°

grid. The results could be enhanced by using Large Eddy Simulation (LES) or Direct Numerical Simulation (DNS), which are able to account for smaller scale turbulence effects, but these have a computational demand many times higher than RANS calculations. Machine learning technologies are beginning to gain ground in the world of numerical simulations, which optimize computation time while maintaining accuracy.

Wind tunnel measurements are necessary to verify the simulation results, calculated in virtual space and to provide more accurate simulation boundary conditions for future calculations.

It would be worthwhile investigating other parameters of the VG geometry and examining the current h and x parameters in more discrete values. Investigation of other Reynolds number ranges, different shapes of VGs and using VGs on different airfoils could also yield interesting results in future work.

References

Anderson, J. D., Cadou, C. P. (2023) "Fundamentals of Aerodynamics", McGraw-Hill Education. ISBN 9781266076442

Ansys, Inc. (2020) "ANSYS Fluent Mosaic Technology Automatically Combines Disparate Meshes with Polyhedral Elements for Fast, Accurate Flow Resolution", [pdf] Ansys, Inc., Canonsburg, PA, USA. Available at: https://www.ansys.com/content/dam/resource-center/white-paper/ansys-fluent-mosaic-technology-wp.pdf [Accessed: 12 September 2024]

Ansys, Inc. (2021) "ANSYS Fluent Theory Guide", [pdf] Ansys, Inc., Canonsburg, PA, USA. Available at: https://dl.cfdexperts.net/cfd_resources/Ansys_Documentation/Fluent/Ansys_Fluent_Theory_Guide.pdf [Accessed: 12 September 2024]

Ansys, Inc. "Ansys Fluent, (2024 R1)", [computer program] Available at: www.ansys.com/products/fluids/ansys-fluent [Accessed: 12 September 2024]

Balaji, K., Gore, M. R., Khandal, S. V. (2023) "Numerical and Experimental Study of Vortex Generator", In: FLAME 2022: Biennial International Conference on Future Learning Aspects of Mechanical Engineering, Noida, India, pp. 249–260. ISBN 978-981-99-3032-6 https://doi.org/10.1007/978-981-99-3033-3_22

Benson, T. (2021) "Boundary Layer", National Aeronautics and Space Administration (NASA), May 13. [online] Available at: https://www.grc.nasa.gov/www/k-12/BGP/boundlay.html [Accessed: 13 May 2021]

De Tavernier, D., Ferreira, C., Viré, A., LeBlanc, B., Bernardy, S. (2021) "Controlling dynamic stall using vortex generators on a wind turbine airfoil", Renewable Energy, 172, pp. 1194–1211. https://doi.org/10.1016/j.renene.2021.03.019

Gao, L., Zhang, H., Liu, Y., Han, S. (2015) "Effects of vortex generators on a blunt trailing-edge airfoil for wind turbines", Renewable Energy, 76, pp. 303–311. https://doi.org/10.1016/j.renene.2014.11.043

Gibertini, G., Boniface, J. C., Zanotti, A., Droandi, G., Auteri, F., Gaveriaux, R., Le Pape, A. (2015) "Helicopter drag reduction by vortex generators", Aerospace Science and Technology, 47, pp. 324–339. https://doi.org/10.1016/j.ast.2015.10.004

Himo, R., Bou-Mosleh, C., Habchi, C. (2021) "Aerodynamic performance enhancement of an Airfoil using trapezoidal vortex generators", Aircraft Engineering and Aerospace Technology, 93(1), pp. 76–84. https://doi.org/10.1108/AEAT-01-2020-0021

Houghton, E. L., Carpenter, P. W., Collicott, S. H., Valentine, D. T. (2016) "Aerodynamics for Engineering Students", Butterworth-Heinemann. ISBN 9780081002322

Katz, J. (1996) "Race Car Aerodynamics: Designing for Speed", Robert Bentley Inc. ISBN 9780837601427

Katz, J. (2021) "Aerodynamics in motorsports", Proceedings of the Institution of Mechanical Engineers, Part P: Journal of Sports Engineering and Technology, 235(4), pp. 324–338. https://doi.org/10.1177/1754337119893226

Li, S., Zhang, L., Xu, J., Yang, K., Song, J., Guo, G. (2020) "Experimental investigation of a pitch-oscillating wind turbine airfoil with vortex generators", Journal of Renewable and Sustainable Energy, 12(6), 063304. https://doi.org/10.1063/5.0013300

Li, T., Liang, H., Zhang, J., Zhang, J. (2023) "Numerical study on aerodynamic resistance reduction of high-speed train using vortex generator", Engineering Applications of Computational Fluid Mechanics, 17(1), e2153925. https://doi.org/10.1080/19942060.2022.2153925

Methal, Z., Talib, A. S. A., Bakar, M. S. A., Rahman, M. R. A., Sulaiman, M. S., Saad, M. R. (2023) "Improving the Aerodynamic Performance of WIG Aircraft with a Micro-Vortex Generator (MVG) in Low-Speed Condition", Aerospace, 10(7), 617. https://doi.org/10.3390/aerospace10070617

Mueller-Vahl, H., Pechlivanoglou, G., Nayeri, C. N., Paschereit, C. O. (2012) "Vortex Generators for Wind Turbine Blades: A Combined Wind Tunnel and Wind Turbine Parametric Study", In: ASME Turbo Expo 2012: Turbine Technical Conference and Exposition, Copenhagen, Denmark, pp. 899–914. ISBN 978-0-7918-4472-4 https://doi.org/10.1115/GT2012-69197

Rohács, J., Gausz, Z., Gausz, T. (2012) "Aerodinamika" (Aerodynamics), Typotex Kiadó. ISBN 978-963-279-614-7 (in Hungarian)

Priyadi, M. U. Z., Syaiful, Muchammad (2022) "Heat Transfer Enhancement in Heat Exchanger using Convex Delta Winglet Vortex Generators", European Journal of Engineering and Technology Research, 7(6), pp. 96–100. http://doi.org/10.24018/ejeng.2022.7.6.2920

Sheikhnejad, Y., Gandjalikhan Nassab, S. A. (2021) "Enhancement of solar chimney performance by passive vortex generator", Renewable Energy, 169, pp. 437–450. https://doi.org/10.1016/j.renene.2021.01.026

Zhang, F., Zuo, Y., Zhu, D., Tao, R., Xiao, R. (2023) "Investigation of Fractal Characteristics of Karman Vortex for NACA0009 Hydrofoil", Fractal and Fractional, 7(6), 467. https://doi.org/10.3390/fractalfract7060467

Zhang, L., Li, X., Yang, K., Xue, D. (2016) "Effects of vortex generators on aerodynamic performance of thick wind turbine airfoils", Journal of Wind Engineering and Industrial Aerodynamics, 156, pp. 84–92. https://doi.org/10.1016/j.jweia.2016.07.013